7-2016

SPICA: stereographic projection for interactive crystallographic analysis

Xingzhong Li
University of Nebraska-Lincoln, xli2@unl.edu

JOURNAL OF APPLIED CRYSTALLOGRAPHY

ISSN: 1600-5767

journals.iucr.org/j

SPICA: stereographic projection for interactive crystallographic analysis

X.-Z. Li

J. Appl. Cryst. (2016). **49**, 1818–1826

JOURNAL OF APPLIED CRYSTALLOGRAPHY

ISSN 1600-5767

SPICA: stereographic projection for interactive crystallographic analysis

X.-Z. Li*

Nebraska Center for Materials and Nanoscience, University of Nebraska, Lincoln, NE 68521, USA. *Correspondence e-mail: xzli@unl.edu

Received 8 April 2016
Accepted 8 July 2016

Edited by Th. Proffen, Oak Ridge National Laboratory, USA

Keywords: stereographic projection; orientation relationships; Kikuchi maps; selected-area electron diffraction; computer programs.

In numerous research fields, especially the applications of electron and X-ray diffraction, stereographic projection represents a powerful tool for researchers. *SPICA* is a new computer program for stereographic projection in interactive crystallographic analysis, which inherits features from the previous *JECP/SP* and includes more functions for extensive crystallographic analysis. *SPICA* provides fully interactive options for users to plot stereograms of crystal directions and crystal planes, traces, and Kikuchi maps for an arbitrary crystal structure; it can be used to explore the orientation relationships between two crystalline phases with a composite stereogram; it is also used to predict the tilt angles of transmission electron microscopy double-tilt and rotation holders in electron diffraction experiments. In addition, various modules are provided for essential crystallographic calculations.

1. Introduction

Stereographic projection is a projection of points from the surface of a sphere onto its equatorial plane. The projection is defined as follows: if a point *P* on the surface of the sphere is joined to the south pole *S* (or the north pole *N*) and the line *PS* (or *PN*) cuts the equatorial plane at *p*, then *p* is the stereographic projection of *P*. The importance of the stereographic projection in crystallography derives from the fact that a set of points on the surface of a sphere provides a complete representation of a set of directions in three-dimensional space, the directions being the set of lines from the center of the sphere to the set of points. A complete stereographic projection of some particular set of points is usually called a stereogram. The mathematics behind the geometry of stereographic projection and the computer implementations are well documented in the literature (*e.g.* Bennett, 1928; Young & Lytton, 1972) and can also be found in most books on electron microscopy and X-ray crystallography (*e.g.* Edington, 1975; Cullity, 1978; De Graef, 2003; Fultz & Howe, 2008).

Stereographic projections of crystal directions and planes are usually the essential modules in most commercial or public domain computer programs for crystallography or electron microscopy: for example, *CaRIne* (Boudias & Monceau, 1998), *Crystallographica* (Siegrist, 1997), *DIAMOND* (Bergerhoff *et al.*, 1996), *CrystalMaker* (Kohn, 1995; Palmer & Palmer, 2016), *Crystal Studio* (Crystalsoftcorp, 2015), *WebEMAP* (Zuo & Mabon, 2004) and *JEMS* (Stadelmann, 1987). As program modules, they are sufficient for regular use to draw stereograms of crystal directions and planes. On the other hand, dedicated computer programs are available for the extended use of stereographic projections. A computer program for simulation of electron diffraction Kikuchi patterns was developed by Lee *et al.* (1994) on the basis of work by Young

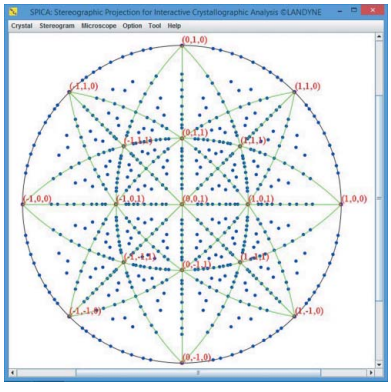

& Lytton (1972). *JECP/SP* (Li, 2004) was developed for generating stereographic projections applicable to specimen orientation adjustment in transmission electron microscopy (TEM) experiments. *SP2* (Liu & Liu, 2012) was developed for standard operation of stereographic projections and can also be used to make composite stereograms, which are necessary to explore the orientation relationships between two crystalline phases.

For crystallographic analysis in electron diffraction experiments, stereographic projection software is expected to include more functions: for example, not only the standard stereogram analysis, but also the composite stereogram for analyzing the relationship of two crystalline phases, the simulation of Kikuchi maps and the prediction of tilt angles in selected-area electron diffraction (SAED) experiments. In the present work, a user-friendly computer program, *SPICA*, has been developed as a dedicated software on stereographic projection, which includes all of the features mentioned above and a few more of its own. *SPICA* can be used as a teaching aid for students in crystallography as well as a practical tool for researchers performing TEM experiments and analysis of the experimental results.

2. Program design and features

SPICA was programmed using Java SE Development Kit 8 (JDK8u74) from Oracle. It has been successfully tested on Microsoft Windows 7, 8 and 10 with a Java virtual machine, *i.e.* Java 2 Runtime Environment (J2RE). The software can be executed as a standalone program or as one component in the *Landyne* software suite with a launcher (Li, 2016), both of which can be downloaded at http://www.unl.edu/ncmn-cfem/xzli/computer-programs.

The graphical user interface (GUI) of *SPICA* utilizes Java Swing to provide a Windows-style operational environment. It consists of a scalable display panel of the stereogram and various dialogs for data input/output and graphics editing operations. Fig. 1 shows the display panel of *SPICA* with the menu bar and an example of a cubic (*hkl*) stereogram with traces indicated of some of the principal zones. Fig. 2 shows three basic operational dialogs in *SPICA*: (*a*) the calculation dialog, (*b*) the pole range dialog, and (*c*) the orientation dialog for the Wulff net and stereograms. More operational dialogs of *SPICA* for other purposes are available (not shown here).

SPICA is a fully functional tool for generating stereograms of crystal directions and planes. To generate a stereogram, the user needs to provide the crystalline lattice parameters, a, b, c, α, β, γ, and the direction of projection, [*uvw*] or (*hkl*). As an option, the Wulff net can be drawn and rotated on top of the generated stereogram. Crystal lattice parameters can be loaded from a data file and readjusted in the calculation dialog (see Fig. 2*a*). Two stereograms from two crystalline phases can be generated and overlaid into a composite stereogram to analyze their structural relationship. The list of (*hkl*) can be edited to show trace curves of selected (*hkl*) poles. Kikuchi maps can be displayed from the generated data of (*hkl*) poles and the wavelength of the incident beam. The zone axes for the Kikuchi maps can be generated from the same crystalline phase on the second stereogram and then overlaid with the

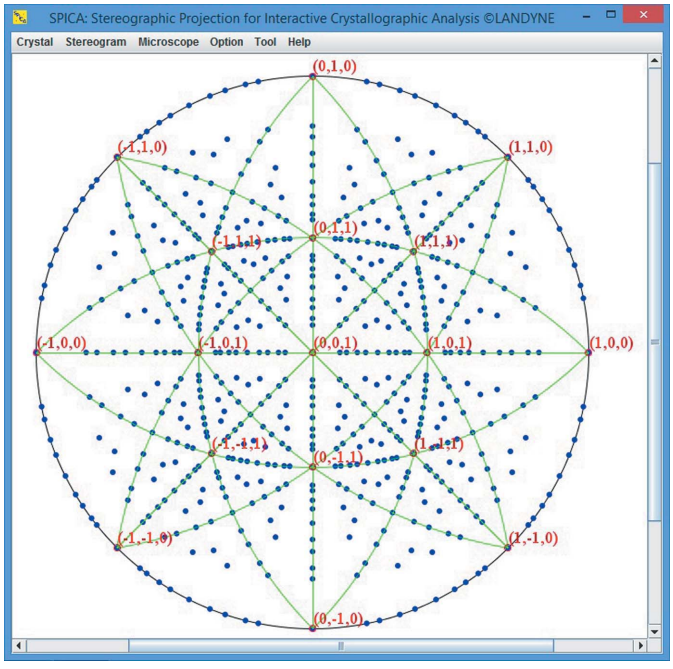

Figure 1
Graphical user interface of *SPICA* with an (*hkl*) stereogram of a cubic structure as an example.

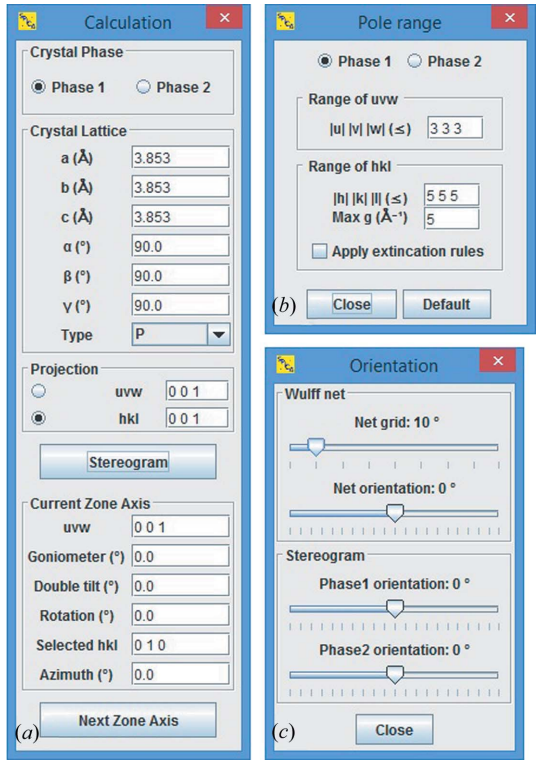

Figure 2
Three basic operational dialogs in *SPICA*: (*a*) the calculation dialog, (*b*) the pole range dialog, and (*c*) the orientation dialog for the Wulff net and stereograms.

Kikuchi map. The additional application is to predict tilt/rotation angles of zone axes for both double-tilt and rotation TEM holders.

3. Crystallographic principles and implementation

As mentioned above, the mathematics behind the geometry of stereographic projection can be found in most books for electron microscopy and X-ray crystallography. There are various ways to implement stereographic projections in computer programs. The implementation in *SPICA* is briefly described in this section.

3.1. Wulff net

The Wulff net, or stereographic net, is a stereographic projection of the longitude and latitude curves on a sphere, which can be drawn as two series of circles with their centers and radii as shown in Fig. 3.

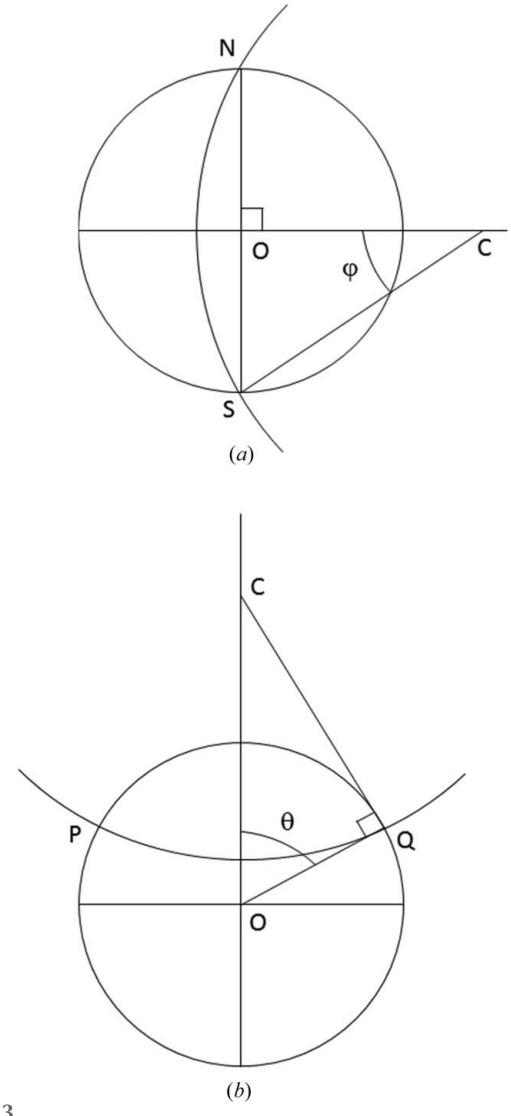

Figure 3
The construction of the Wulff net: (*a*) the longitude and (*b*) the latitude curves on a sphere.

Longitude arcs:

$$y^2 + (x \pm r/\tan\varphi)^2 = (r/\sin\varphi)^2. \quad (1a)$$

Latitude arcs:

$$(y \pm r/\cos\theta)^2 + x^2 = (r\tan\theta)^2. \quad (1b)$$

Here r is the radius of the sphere of the stereogram. The coordinates (x, y) are on the longitude or latitude circles. The above formulas can be derived from the definition of the Wulff net.

3.2. Stereographic projection

The orthogonal Cartesian coordinate system for a crystal lattice is set up as follows: The c axis of a crystal lattice is oriented along the z axis of the coordinate system, and the a axis is set up in the xz plane. The orientation of the b axis is then fixed so as to maintain right handedness, and the coordinates of the a and b axes calculated. A stereogram is first calculated using (001) or [001] as the initial direction of projection. The stereogram with a specific direction of projection, (*hkl*) or [*uvw*], is obtained by rotating the initial

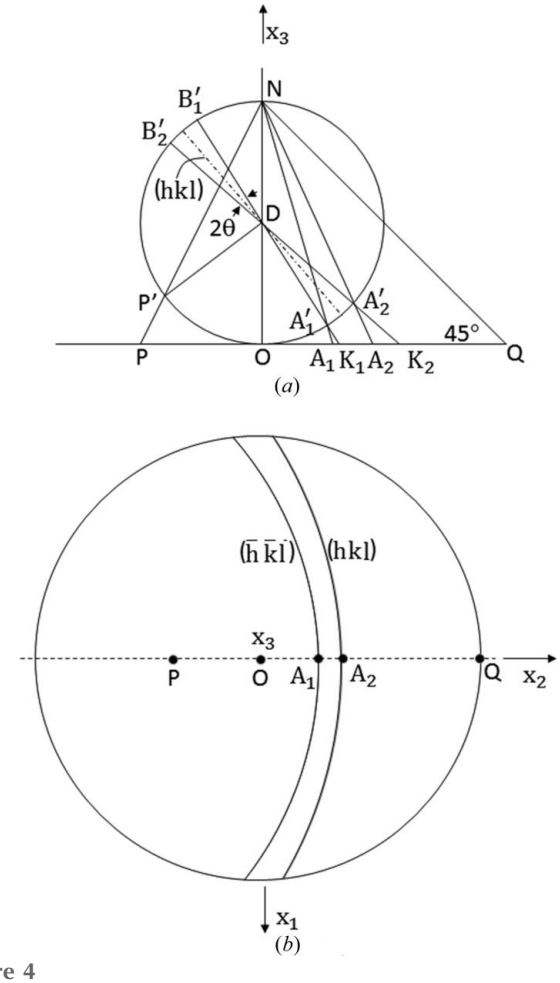

Figure 4
The geometric construction of a Kikuchi map by stereographic projection.

stereogram so that (*hkl*) or [*uvw*] becomes the direction of projection.

Fig. 4(*a*) shows a sphere with its center at *D* and a plane passing though *O* for stereographic projection. This plane works the same as the equatorial plane in the definition; the projected diagram is enlarged (×2) in this case. The projection from the north pole and through the equator of the sphere to the stereographic plane is *NQ*. It defines a circle with a radius of *OQ* on the stereographic plane. For any point *P* on the stereographic plane, a line *NP* intersects the sphere at one point *P*′. *NP* defines the stereographic projection of *P*′ to *P* on the stereographic plane. In Cartesian coordinates, (*x*, *y*, *z*) are the coordinates on the sphere and (*X*, *Y*) are the coordinates on the plane. The relationship between the projection point on the stereographic plane and the associated point on the sphere is given by the formula

$$(X, Y) = \left(\frac{x}{1-z}, \frac{y}{1-z}\right). \tag{2}$$

Here the set of points (*x*, *y*, *z*) are on a unit sphere, so that $x^2 + y^2 + z^2 = 1$.

3.3. Composite stereogram

SPICA allows two stereograms either from the same or from different crystalline phases to be generated simultaneously; either the two single stereograms or the overlaid stereogram can be displayed separately. Both the stereogram and the Wulff net can be rotated by stepwise increments of 0.01° in order to analyze the crystallographic relationship. If the stereograms are generated from the same crystalline phase, different features can be displayed: *e.g.* one may show plane traces while the other shows poles corresponding to the same set of plane indices; one shows the plane (*hkl*) poles and the other shows the [*uvw*] poles; or one shows a Kikuchi map and the other shows the [*uvw*] poles.

3.4. Kikuchi map and trace curve

Although the Kikuchi patterns obtained using TEM are not truly stereographic projections, they are excellent approximations to them when the camera length is relatively large (Young & Lytton, 1972). Furthermore, the use of the stereographic projection in simulated patterns allows the display of all possible orientations on a single figure, which cannot be done easily with a photographic montage.

The coordinate system for generating a Kikuchi map in stereographic projection was adopted from the work of Young & Lytton (1972). The geometry for the standard stereographic projection of a Kikuchi line pair is shown in Fig. 4; (*b*) is the projection of (*a*) with the observer looking from *N* toward *O*. Here the projected plane normal $P(P_x, P_y)$ can be calculated from the following equations:

$$P_x = (2DO)\tan\left(\tfrac{1}{2}\gamma\right)P'_x/(P'^2_x + P'^2_y)^{1/2}, \tag{3a}$$

$$P_y = (2DO)\tan\left(\tfrac{1}{2}\gamma\right)P'_y/(P'^2_x + P'^2_y)^{1/2}, \tag{3b}$$

$$\gamma = \cos^{-1}[P'_z/(P'^2_x + P'^2_y + P'^2_z)]^{1/2}, \tag{3c}$$

where P'_x, P'_y and P'_z are the coordinates of P' $[r = (P'^2_x + P'^2_y + P'^2_z)^{1/2}]$ referred to the standard basis for stereographic projection, and γ is the angle between the plane normal DP' and DO. The formulas above can be used to generate trace curves by applying $\theta = 0°$.

The Kikuchi map is generated from the data set of the (*hkl*) stereographic projection, and the distribution of the zone axes on the Kikuchi map can be found from the [*uvw*] stereographic projection of the same crystal phase on the second stereogram. For a cubic crystal, the plane normal is parallel to the orientation with the same index as this plane, but it is necessary to transform between the plane index and the plane normal index for non-cubic crystals. A function for the transformation from a plane (*hkl*) to the plane normal [*uvw*] is provided in *SPICA* on the basis of the work by Liu & Liu (2012).

3.5. Prediction of the tilt or rotation angles for a TEM holder

Computer-assisted specimen orientation adjustment in TEM experiments is possible for a crystalline specimen with known lattice parameters. The microscope can be kept in the image mode while the specimen is tilted to any zone axis within the range available for the TEM specimen holder under calculated guidance. The application of stereographic projection for specimen orientation adjustment was described in the paper by Chou (1987). A slightly different algorithm was adopted in *JECP/SP* and inherited in *SPICA*.

The key point is to set up the positions of the TEM specimen holder and the crystal orientation in the stereographic projection sphere. The tilt angle of the TEM goniometer and the second tilt angle are assumed to be along the longitude and latitude of the stereographic projection sphere. The crystal orientation can be obtained from the observed SAED pattern. Suppose that the SAED pattern with a zone axis [*uvw*] is currently observed. For any diffraction spot (*hkl*) on the SAED pattern, the azimuth χ is between the line of (000)–(*hkl*) and the projection of the TEM specimen holder (or goniometer axis) on the fluorescent screen, as shown in Fig. 5. A stereographic projection map can be calculated using the above input parameters to provide all the zone axes with

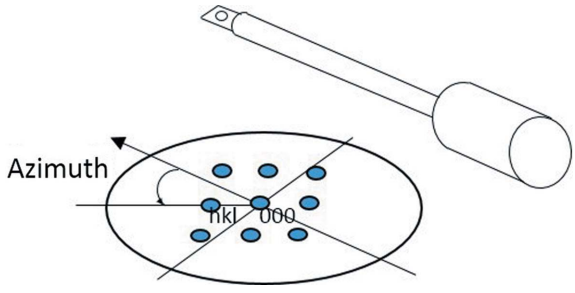

Figure 5
The geometric relation of the observed SAED pattern and the TEM specimen holder for a stereographic projection as guidance in SAED experiments.

calculated tilt or rotation angles. The tilt limitation of the TEM holder can also be drawn in the generated stereogram.

3.6. Modules for crystallographic calculation

One module mentioned above is for the transformation from the crystal plane (*hkl*) to the plane normal [*uvw*] for non-cubic crystalline phases. Other modules include the calculation of (i) the angle between two crystal planes, (ii) the angle between two zone axes, (iii) the angle between a plane normal and a zone axis, (iv) the transformation between Miller and Miller–Bravais indices for the hexagonal system, and (v) a calculated list of reflections (*hkl*), together with the plane spacing and the kinematical intensity.

4. Comparison of *SPICA* with *SP2*

SP2 (Liu & Liu, 2012) is a recent computer program for stereographic projection. A comparison between *SP2* and *SPICA* is given here.

A composite stereogram is useful in analyzing the mutual orientation relationship between two crystalline phases. All possible orientation relationships can be found on the composite stereogram, which is a valuable guide for users to measure habit plane and growth orientations. Both *SPICA* and *SP2* provide a function for overlaid stereograms. Although the implementation of this function in *SPICA* and *SP2* may be different, the result is the same; see an example of the composite stereogram in next section.

SP2 provides the option to show a Kikuchi map as a stereogram generated with high-index orientation vectors (zone axes). However, this oversimplified solution has some limitations: (*a*) it does not show the width of the Kikuchi band, which is determined by the wavelength of the incident beam, and (*b*) it requests the extinction rules in the stereogram for non-primitive (*e.g.* body-centered cubic and face-centered cubic) lattices. It is known that the Kikuchi maps of the three lattices are different but the [*uvw*] stereographic projections of the three lattices are the same. *SPICA* adopts the formula developed by Young & Lytton (1972), which allows us to easily simulate the Kikuchi, electron backscatter diffraction (EBSD), and Kossel or pseudo-Kossel patterns by changing the wavelength of the incident beam. This method is more practical than the method used by *SP2*. One of the overlaid stereograms can also be used for providing information on the zone axes in *SPICA*.

The implementation of the trace of a plane in a stereogram is available in both *SPICA* and *SP2*. The plotting method for the trace of a plane is similar to that for the Wulff net in *SP2*, while the formula for the Kikuchi curve above is used with the Bragg angle = 0° in *SPICA*. *SP2* introduces a function to show the triangular zone of the pole figure. A similar triangular zone can be generated by selected trace lines in *SPICA*. In addition, *SPICA* provides the prediction of the tilt angles for each zone axis within the the tilt range of the TEM double-tilt or rotation holder.

5. Application examples

Some application examples are given here to show the proof of validity and practicability of *SPICA*. The basic usage steps are introduced here; more details are given in the user manual of *SPICA*.

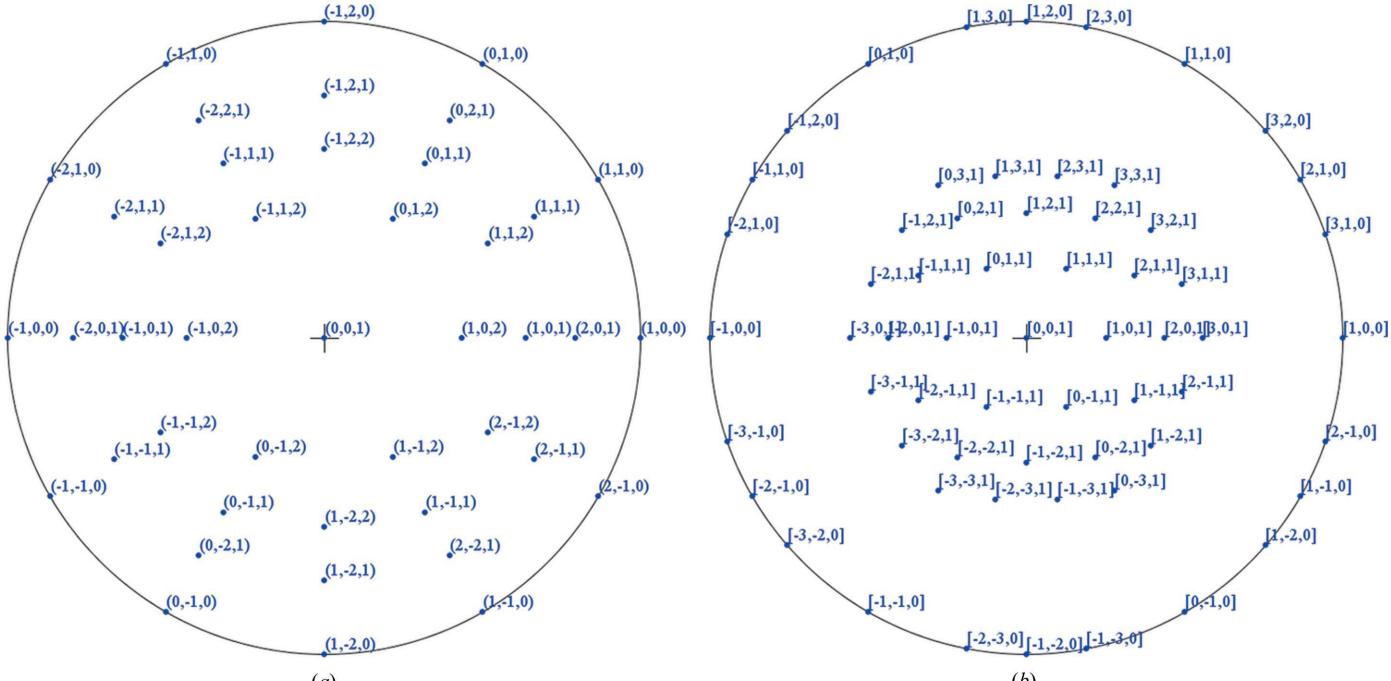

Figure 6
Stereogram of the hexagonal structure of Zn: (*a*) (*hkl*) stereogram and (*b*) [*uvw*] stereogram. In order to display clearly all indices, the maximum indices were set to $h \leq 2$, $k \leq 2$, $l \leq 2$, $u \leq 3$, $v \leq 3$ and $w \leq 1$.

5.1. Stereogram and Wulff net

The input parameters to generate a stereogram include the lattice parameters of a crystalline phase and the direction of projection. The lattice parameters can be loaded from a crystal structure file using the menu bar and can be readjusted in the calculation dialog, if necessary. The range of the poles is adjustable using the pole range dialog. When a list of the poles is generated, any pole in the list can be deleted or a new one can be added to the list. The stereogram and the Wulff net can be rotated separately. The display of the stereogram can be zoomed in or out. Fig. 6 shows (*a*) the (*hkl*) stereogram and (*b*) the [*uvw*] stereogram of the hexagonal structure of Zn, a = 0.26649, b = 0.26649, c = 0.49468 nm, $\alpha = 90$, $\beta = 90$, $\gamma = 120^\circ$. In order to display all indices clearly, the maximum indices were chosen as $h \le 2$, $k \le 2$, $l \le 2$, $u \le 3$, $v \le 3$ and $w \le 1$. The Miller index is labeled in the stereogram; the Miller–Bravais index can be transformed from the Miller index using a module in *SPICA*. The Wulff net, as a tool for measurement, can be applied to the stereogram by users. The Wulff net is applied in Fig. 1 and not applied in Fig. 6.

5.2. Composite stereogram

Two sets of stereograms can be generated separately and rendered together to show a composite stereogram, which can be used to explore all possible well matching pairs between the planes or the orientations for two crystalline phases with a fixed orientation relationship. Fig. 7 shows the typical Burgers orientation relationship between a hexagonal close-packed matrix and a body-centered cubic precipitate in the α-Mg/γ-$Mg_{17}Al_{12}$ precipitation system. The Burgers (1934) orientation relationship can be expressed as

$$(001)_\alpha // (110)_\gamma \quad [100]_\alpha // [\bar{1}11]_\gamma \quad [\bar{1}\bar{2}0]_\alpha // [\bar{1}\bar{1}2]_\gamma$$

or in the Miller–Bravais system for the hexagonal phase as

$$(0001)_\alpha // (110)_\gamma \quad [2\bar{1}\bar{1}0]_\alpha // [\bar{1}11]_\gamma \quad [0\bar{1}10]_\alpha // [\bar{1}\bar{1}2]_\gamma.$$

The composite stereogram is plotted by drawing stereographic projections viewed at [001] and [110] orientations for the matrix and precipitate, respectively. Fig. 7 shows two identical stereograms with (*a*) the index labels of the α-Mg phase and (*b*) the index labels of the γ-$Mg_{17}Al_{12}$ phase. The same example was used in the article on *SP2* (Liu & Liu, 2012).

The second example is taken from our recent work on $Mn_2CrGa_{1-x}Al_x$ alloys, x = 0.0, 0.2, 0.5 (Li *et al.*, 2016). A spinodal decomposition of the alloys (x = 0.2, 0.5) generates two crystalline phases with a fixed orientation relationship after an annealing treatment at 773 K for 2 h. The lattice parameters of the two phases in the $Mn_2CrGa_{0.5}Al_{0.5}$ alloy are listed in Table 1. Fig. 8(*a*) shows a TEM image of the two

Table 1
Lattice parameters of the crystalline phases in the application examples.

The compositions were measured by energy dispersive spectrometry.

Composition	Lattice type	a (nm)	b (nm)	c (nm)	Reference
$Mn_{63}Cr_{11}Ga_{13}Al_{13}$	Cubic	0.645	0.645	0.645	Li *et al.* (2016)
$Mn_{45}Cr_{31}Ga_{13}Al_{11}$	Tetragonal	0.295	0.295	0.87	Li *et al.* (2016)
$Co_{39}Fe_{42}Cr_9Ge_{10}$	Tetragonal	0.76	0.76	0.284	Jin *et al.* (2016)

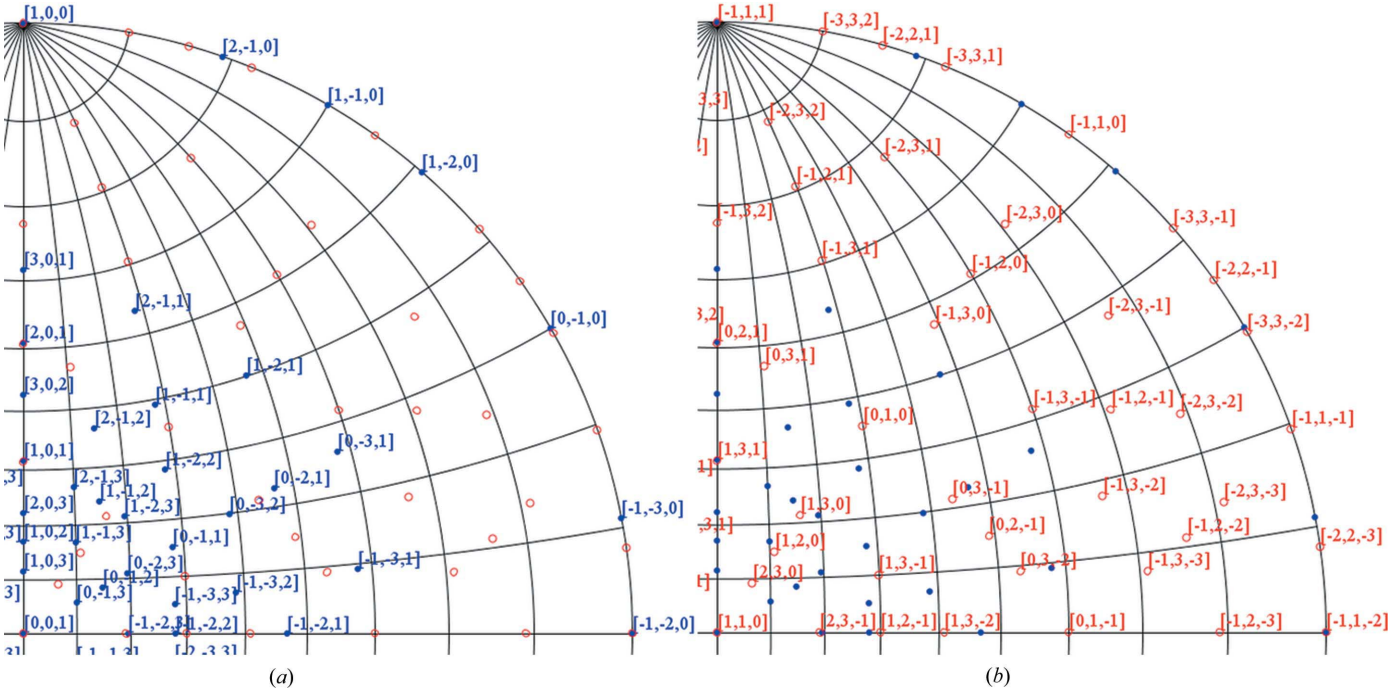

Figure 7
Composite stereogram of the typical Burgers orientation relationship between the matrix and precipitate in the α-Mg/γ-$Mg_{17}Al_{12}$ precipitation system.

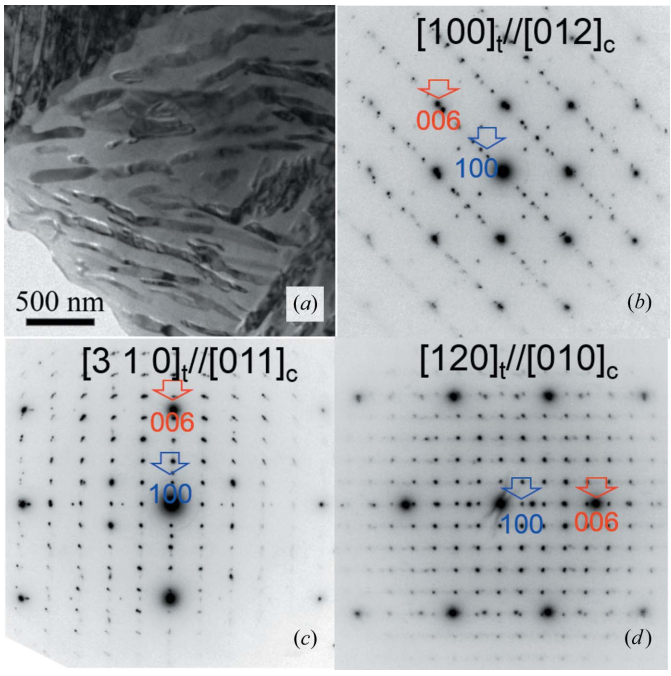

Figure 8
Two crystalline phases in the $Mn_2CrGa_{0.5}Al_{0.5}$ alloy, resulting from a spinodal decomposition: (*a*) a TEM image of the two phases (cubic phase in light grey and tetragonal phase in dark-grey strips), and (*b*)–(*d*) the electron diffraction patterns taken from the two crystalline phases.

crystalline phases in the $Mn_2CrGa_{0.5}Al_{0.5}$ alloy; the cubic phase, in light grey, has a composition of $Mn_{63}Cr_{11}Ga_{13}Al_{13}$ and the tetragonal phase, appearing as strips of dark grey, has a composition of $Mn_{45}Cr_{31}Ga_{13}Al_{11}$. Figs. 8(*b*)–8(*d*) show the SAED patterns to reveal the orientation relationship of the two crystalline phases. Fig. 9 shows the composite stereograms with (*a*) the index labels of the cubic phase and (*b*) the index labels of the tetragonal phase. The fixed orientation relationship of the two crystalline phases is

$$(001)_t//(100)_c \quad [100]_t//[012]_c \quad [310]_t//[011]_c \quad [120]_t//[010]_c.$$

5.3. Kikuchi map and trace curve

The Kikuchi map is displayed by first generating a stereogram of (*hkl*) and then selecting the corresponding display mode in *SPICA*. The additional parameter for the Kikuchi map is the wavelength of the incident beam or the accelerating voltage of the transmission electron microscope. Fig. 10 shows the Kikuchi maps of a primitive cubic structure with the [111] zone axis in the center, (*a*) generated using the method described by Liu & Liu (2012) and (*b*) generated using the formula of Young & Lytton (1972) with a wavelength of 0.0251 Å (200 kV). The overlaid distribution of the [*uvw*] zone axes is shown in Fig. 10(*b*).

Similar to the Kikuchi map, the Kossel map in X-ray diffraction and the EBSD map can also be simulated with *SPICA* by selecting an appropriate wavelength. The trace curve is displayed by generating a stereogram of (*hkl*) and then selecting the corresponding mode; one example was shown in Fig. 1.

5.4. Tilt-angle prediction for a TEM holder

This function is very useful in many situations, for example (*a*) when a severely strained specimen is observed and the visibility of Kikuchi line pairs is thus poor; (*b*) when a beam-sensitive specimen is examined, and it is essential to shorten the time spent on specimen tilting while the electron beam is on the specimen area of interest; (*c*) when a small-grain-size

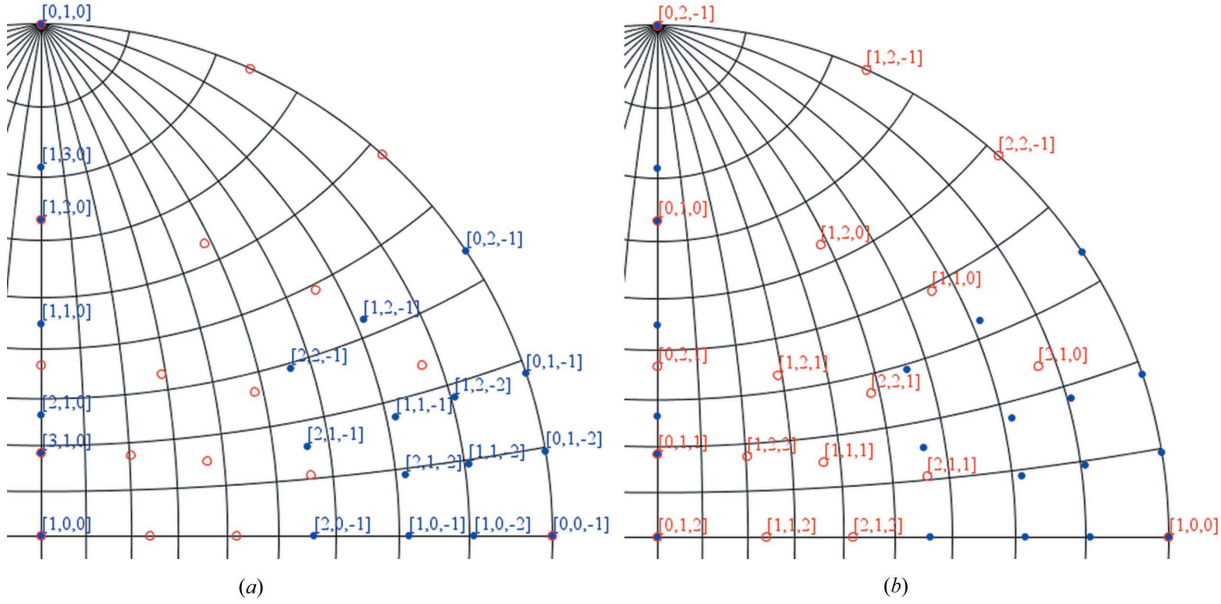

Figure 9
Composite stereogram for the $Mn_2CrGa_{0.5}Al_{0.5}$ alloy with (*a*) the index labels for the cubic phase and (*b*) the index labels for the tetragonal phase.

specimen is investigated, for which even a slight orientation adjustment may cause the corresponding diffraction pattern to disappear owing to a lateral sample shift; and (*d*) when a crystalline specimen is used in acquiring electron diffraction intensities of reachable zone-axis patterns for structure determination.

An example is the electron diffraction experiment for a new tetragonal phase with the composition $Co_{39}Fe_{42}Cr_9Ge_{10}$ in our

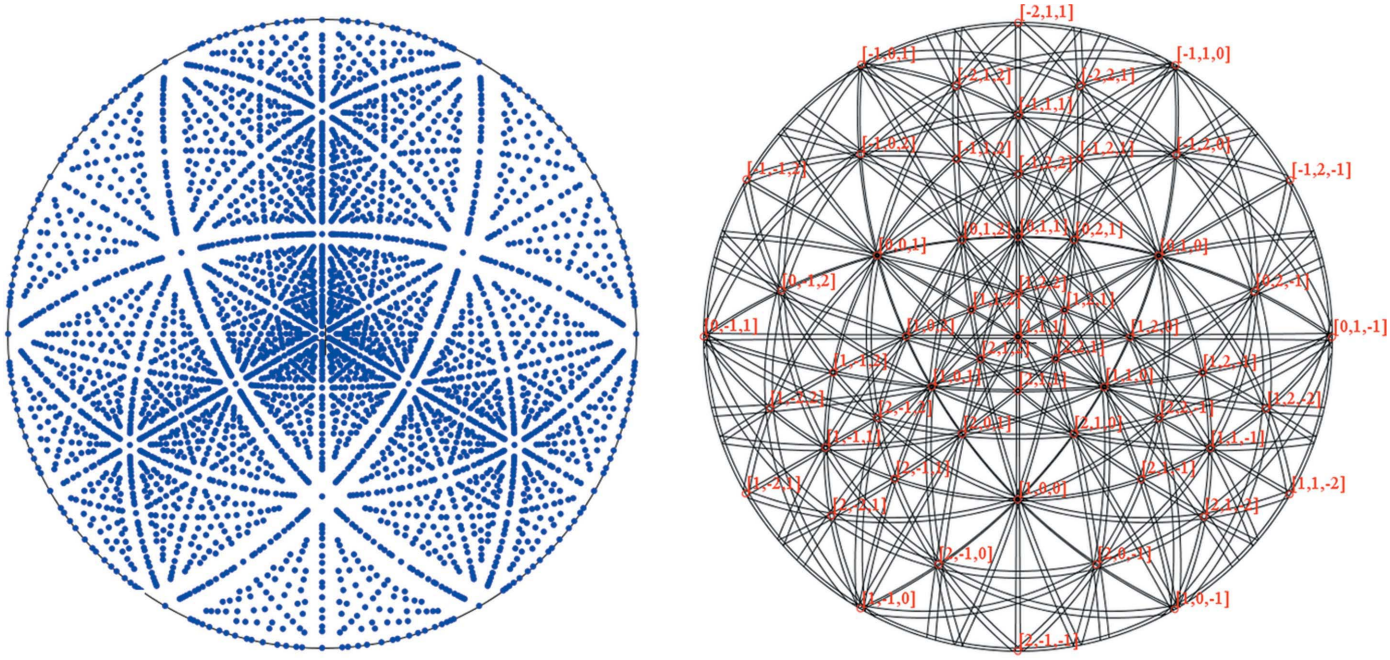

Figure 10
Kikuchi maps of a primitive cubic structure with the [111] zone axis in the center, (*a*) generated using the method described by Liu & Liu (2012) and (*b*) generated using the formula of Young & Lytton (1972) with a wavelength of 0.0251 Å (200 kV).

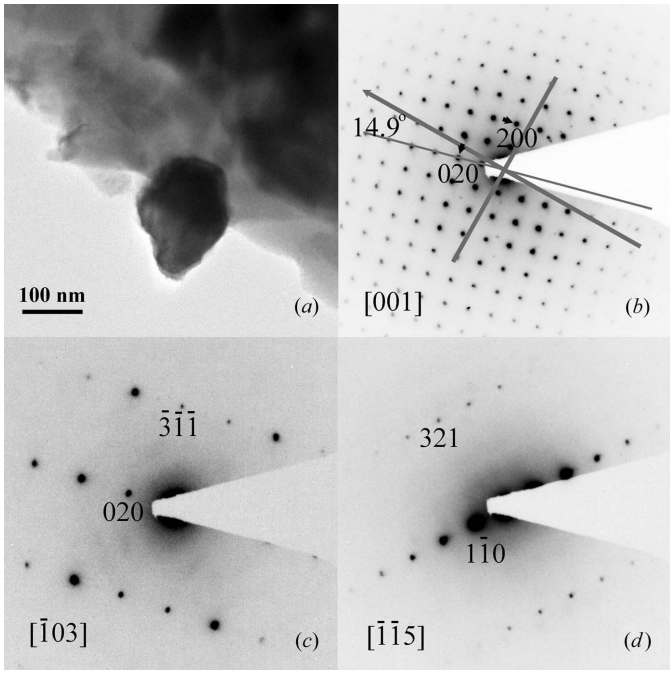

Figure 11
A new tetragonal phase in an Co–Fe–Cr–Ge alloy. (*a*) TEM image of the tetragonal phase with a grain size of about 150 nm, and (*b*)–(*d*) SAED patterns of the tetragonal phase.

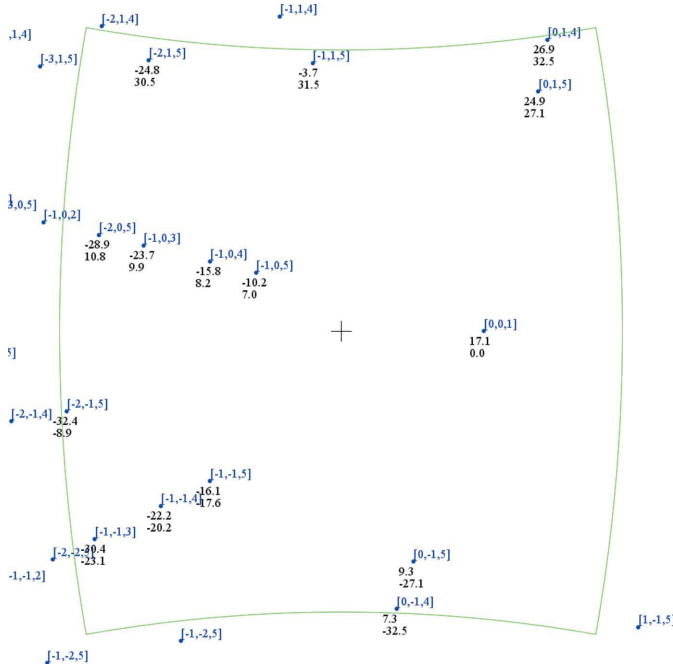

Figure 12
The new tetragonal phase in the Co–Fe–Cr–Ge alloy as an example of using *SPICA* to predict the tilt angles for all zone axes within the tilt limitations of the TEM specimen holder. The SAED patterns of the [$\bar{1}$03] and [$\bar{1}\bar{1}$5] zone axes were selected, and these are displayed in Fig. 11(*c*) and 11(*d*).

recent work (Jin *et al.*, 2016); the lattice parameters are listed in Table 1. Fig. 11 shows (*a*) a TEM image of the new tetragonal phase with a grain size about 150 nm, and (*b*)–(*d*) SAED patterns of the new tetragonal phase. In the experiment, the [001] SAED pattern in Fig. 11(*b*) was obtained at tilt angles of (17.1, 0.0°) with a double-tilt TEM holder. The angle between the vector (000)–(010) and the holder axis is about 14.9°. Fig. 12 was generated using *SPICA* with the above parameters to predict the tilt angles for all zone axes within the tilt range of the TEM holder. The TEM specimen was tilted according to the predicted tilt angles and corresponding SAED patterns were obtained. SAED patterns for the $[\bar{1}03]$ and $[\bar{1}\bar{1}5]$ zone axes are displayed in Figs. 11(*c*) and 11(*d*). It should be pointed out that the forbidden reflection, *i.e.* (010), in Fig. 11(*c*) appears in Fig. 11(*d*) owing to the double diffraction effect.

6. Concluding remarks

In summary, *SPICA* is a new dedicated computer program to perform stereographic projection for an interactive crystallographic analysis. It provides all the necessary functions of a stereogram for a single-crystalline phase, including the standard stereogram, trace curve and Kikuchi map. It can display composite stereograms, which are generated either from two different crystalline phases with a fixed crystallographic relationship or from the same crystalline phase for complementary stereographic features. It can also predict the tilt or rotation angles of the zone axes of the TEM holder, thus minimizing the difficulties for highly beam-sensitive and/or small-grain-size specimens with known structures using either a double-tilt or a rotation TEM holder.

Acknowledgements

I gratefully thank Jaimie Iuranich for help in improving the manuscript. I thank my colleagues, especially Wenyong Zhang and Yunlong Jin, for co-working on the $Mn_2CrGa_{0.5}Al_{0.5}$ and Co–Fe–Cr–Ge alloy systems.

References

Bennett, T. (1928). *Am. Math. Mon.* **35**, 24–27.
Bergerhoff, G., Berndt, M. & Brandenburg, K. (1996). *J. Res. Natl Inst. Stand. Technol.* **101**, 221–225.
Boudias, C. & Monceau, D. (1998). *CaRIne Crystallography*. Version 3.1. CaRIne Crystallography, Senlis, France.
Burgers, W. (1934). *Physica*, **1**, 561–586.
Chou, C. T. (1987). *J. Electron. Microsc. Tech.* **7**, 263–268.
Crystalsoftcorp (2015). *Crystal Studio*, http://www.crystalsoftcorp.com.
Cullity, B. D. (1978). *Elements of X-ray Diffraction*. London: Addison-Wesley.
De Graef, M. (2003). *Introduction to Conventional Transmission Electron Microscopy*. Cambridge University Press.
Edington, J. W. (1975). *Electron Diffraction in the Electron Microscope*. London: Macmillan Press.
Fultz, B. & Howe, J. (2008). *Transmission Electron Microscopy and Diffractometry of Materials*. Berlin, Heidelberg: Springer Verlag.
Jin, Y. L., Li, X. Z., Kharel, P., Shah, V. R., Skomski, R. & Sellmyer, D. J. (2016). *A New Tetragonal Phase in Co–Fe–Cr–Ge Alloy*. In preparation.
Kohn, S. C. (1995). *Terra Nova*, **7**, 554–556.
Lee, W.-B., Park, C.-R., Park, C.-G. & Chun, C.-H. (1994). *Korean J. Electron. Microsc.* **24**, 115–122.
Li, X. Z. (2004). *J. Appl. Cryst.* **37**, 506–507.
Li, X. Z. (2016). *Microsc. Microanal.* **22**(Suppl. 3), 564–565.
Li, X. Z., Zhang, W. Y. & Sellmyer, D. J. (2016). *A TEM Study of the Spinodal Decomposition in $Mn_2CrGa_{0.5}Al_{0.5}$ Alloy*. In preparation.
Liu, H. & Liu, J. (2012). *J. Appl. Cryst.* **45**, 130–134.
Palmer, D. C. & Palmer, S. E. (2016). *CrystalMaker*. CrystalMaker Software Ltd, Oxford, UK, http://www.CrystalMaker.com.
Siegrist, T. (1997). *J. Appl. Cryst.* **30**, 418–419.
Stadelmann, P. (1987). *Ultramicroscopy*, **21**, 131–145.
Young, C. T. & Lytton, J. L. (1972). *J. Appl. Phys.* **43**, 1408–1417.
Zuo, J. M. & Mabon, J. C. (2004). *Microsc. Microanal.* **10**, 1000–1001.